

# Optical and Near-Infrared Polarimetry for a Highly Dormant Comet 209P/LINEAR

Daisuke KURODA

*Okayama Astrophysical Observatory, National Astronomical Observatory of Japan,  
Asakuchi, Okayama 719-0232, Japan*

Masateru ISHIGURO

*Department of Physics and Astronomy, Seoul National University, Gwanak, Seoul 151-742,  
Korea*

Makoto WATANABE

*Department of Cosmosciences, Graduate School of Science, Hokkaido University, Kita-ku,  
Sapporo 060-0810, Japan*

Hiroshi AKITAYA<sup>†</sup>

*Hiroshima Astrophysical Science Center, Hiroshima University, Higashihiroshima,  
Hiroshima 739-8526, Japan*

Jun TAKAHASHI

*Nishi-Harima Astronomical Observatory, Center for Astronomy, University of Hyogo,  
Sayo, Hyogo 679-5313, Japan*

Sunao HASEGAWA

*Institute of Space and Astronautical Science (ISAS), Japan Aerospace Exploration Agency  
(JAXA), Sagamihara, Kanagawa 252-5210, Japan*

Takahiro UI, Yuka KANDA, Katsutoshi TAKAKI, Ryosuke ITOH

*Department of Physical Science, Hiroshima University, Higashihiroshima, Hiroshima  
739-8526, Japan*

Yuki MORITANI<sup>‡</sup>

*Kavli Institute for the Physics and Mathematics of the Universe (WPI), The University of  
Tokyo, 5-1-5, Kashiwanoha, Kashiwa, 277-8583, Japan*

Masataka IMAI, Shuhei GODA

*Department of Cosmo sciences, Graduate School of Science, Hokkaido University, Kita-ku,  
Sapporo 060-0810, Japan*

Yuhei TAKAGI, Kumiko MORIHANA, Satoshi HONDA

*Nishi-Harima Astronomical Observatory, Center for Astronomy, University of Hyogo,  
Sayo, Hyogo 679-5313, Japan*

Akira ARAI<sup>§</sup>

*Koyama Astronomical Observatory, Kyoto Sangyo University, Motoyama, Kamigamo,  
Kita-ku, Kyoto 603-8555, Japan*

Hidekazu HANAYAMA

*Ishigakijima Astronomical Observatory, National Astronomical Observatory of Japan,  
1024-1 Arakawa, Ishigaki, Okinawa 907-0024, Japan*

Takahiro NAGAYAMA

*Graduate School of Science and Engineering, Kagoshima University, Kagoshima 890-0065,  
Japan*

Daisaku NOGAMI

*Department of Astronomy, Graduate School of Science, Kyoto University, Kyoto 606-8502,  
Japan*

Yuki SARUGAKU

*Kiso Observatory, Institute of Astronomy, School of Science, The University of Tokyo,  
Kiso-gun, Nagano 397-0101, Japan*

Katsuhiro MURATA

*Department of Astrophysics, Nagoya University, Chikusa-ku, Nagoya 464-8602, Japan*

Tomoki MOROKUMA

*Institute of Astronomy, Graduate School of Science, The University of Tokyo, Mitaka,  
Tokyo 181-0015, Japan*

Yoshihiko SAITO

*Department of Physics, Tokyo Institute of Technology, Meguro-ku, Tokyo 152-8551, Japan*

Yumiko OASA

*Faculty of Education, Saitama University, Sakura, Saitama 338-8570, Japan*

Kazuhiro SEKIGUCHI, Jun-ichi WATANABE

*National Astronomical Observatory of Japan, Mitaka, Tokyo 181-8588, Japan*

## ABSTRACT

We conducted an optical and near-infrared polarimetric observation of the highly dormant Jupiter-Family Comet, 209P/LINEAR. Because of its low activity, we were able to determine the linear polarization degrees of the coma dust particles and nucleus independently, that is  $P_n=30.3^{+1.3}_{-0.9}\%$  at  $\alpha=92.2^\circ$  and  $P_n=31.0^{+1.0}_{-0.7}\%$  at  $\alpha=99.5^\circ$  for the nucleus, and  $P_c=28.8^{+0.4}_{-0.4}\%$  at  $\alpha=92.2^\circ$  and  $29.6^{+0.3}_{-0.3}\%$  at  $\alpha=99.5^\circ$  for the coma. We detected no significant variation in  $P$  at the phase angle coverage of  $92.2^\circ$ – $99.5^\circ$ , which may imply that the obtained polarization degrees are nearly at maximum in the phase-polarization curves. By fitting with an empirical function, we obtained the maximum values of linear polarization degrees  $P_{\max}=30.8\%$  for the nucleus and  $P_{\max}=29.6\%$  for the dust coma. The  $P_{\max}$  of the dust coma is consistent with those of dust-rich comets. The low geometric albedo of  $P_v=0.05$  was derived from the slope–albedo relationship and was associated with high  $P_{\max}$ . We examined  $P_{\max}$ –albedo relations between asteroids and 209P, and found that the so-called Umov law seems to be applicable on this cometary surface.

*Subject headings:* comets: individual (209P/LINEAR) — polarization — meteorites, meteors, meteoroids

---

<sup>†</sup>Core of Research for the Energetic Universe, Hiroshima University, Higashi-Hiroshima, Hiroshima 739-8526, Japan

<sup>‡</sup>Hiroshima Astrophysical Science Center, Hiroshima University, Higashi-Hiroshima, Hiroshima 739-8526, Japan

<sup>§</sup>Nishi-Harima Astronomical Observatory, Center for Astronomy, University of Hyogo, Sayo, Hyogo 679-5313, Japan

## 1. Introduction

The linear polarization of light scattered by airless solar system objects (i.e. comets and asteroids) is a useful tool for investigating the physical properties of their surfaces. The phase-polarization curves display a common behaviour, having a negative polarization branch at  $0^\circ < \alpha \lesssim 20^\circ$ , positive branch at  $\alpha \gtrsim 20^\circ$ , and maximum polarization around  $\alpha = 90^\circ$ – $100^\circ$ , where  $\alpha$  denotes the solar phase angle (i.e. Sun–object–observer’s angle). The phase-polarization curves of asteroids, usually observed in the mainbelt at a low phase angle ( $\alpha < 30^\circ$ ), provide information about composition (i.e. taxonomic type), optical properties, porosity of the surface regolith layers, and so on (see e.g. Dollfus et al. 1989; Shkuratov et al. 2002; Gil-Hutton et al. 2014). In contrast, comets, which are usually enclosed in a dust coma plus gas contamination, have been observed with polarimeters at a wide range of phase angles, providing the composition, size and structure (fluffy or compact) of dust grains in comae (Zubko et al. 2011; Kolokolova et al. 2007).

Although several near-Earth asteroids (NEAs) and active comets were observed at large phase angles, little is known about the polarimetric properties of bare comet nuclei at large phase angles. Whenever comets are observed at large phase angles (i.e.  $\alpha > 90^\circ$ ), their nuclei are supposed to be shrouded in thick cometary comae, because comets are located within 1 AU in the geometry where they are heated up, creating outflow of dust particles and sublimating ice. This paper attempted to obtain unique data of the linear polarization degree,  $P$ , for a bare cometary nucleus as well as dust particles of 209P/LINEAR (hereafter 209P). The comet is classified among the Jupiter-Family Comets (hereafter JFCs, the semimajor axis  $a = 2.932$  AU, eccentricity  $e = 0.692$ , inclination  $i = 19.4^\circ$ , and the Tisserand parameter with respect to Jupiter,  $T_J = 2.80$ ) and known as the parent body of a meteor shower, the May Camelopardalids (Jenniskens & Lyytinen 2014). It closely encountered the Earth in late May, 2014, providing us with the opportunity to observe it at large phase angles. Ishiguro et al. (2015) noticed that 209P nucleus was largely mantled by the surface dust layer, showing very weak activity when it closely approached Earth in 2014 April–May.

We conducted polarimetric observations of the comet at large phase angles in optical and near-infrared wavelengths using newly developed instruments as part of *OISTER* (an inter-university observation network in the optical and infrared wavelengths) activities. From the observed data, we subtracted the faint coma components to derive the nuclear  $P_n$ , and compare the results with those of previous studies.

## 2. Observations and Reductions

### 2.1. Observations

Polarimetric observations of 209P were conducted for five nights in 2014 April–May using two telescopes: the Hiroshima Optical and Near-InfraRed camera (HONIR) on the 1.5-m Kanata telescope (hereafter Kanata) at the Higashi-Hiroshima Astronomical Observatory, Hiroshima, and the visible Multi-Spectral Imager (MSI) on the 1.6-m Pirka telescope (Pirka) at Hokkaido University’s Nayoro Observatory in Hokkaido, Japan. In the imaging polarimetric mode, each instrument employs a Wollaston prism beam-splitter and a rotatable half-wave plate modulator, which produces reliable data sets taking ordinary and extraordinary images simultaneously at four position angles  $\theta=0^\circ$ ,  $45^\circ$ ,  $22.5^\circ$ , and  $67.5^\circ$ . HONIR provides a simultaneous optical and near-infrared imaging polarimetry in a sequence of exposures. The detectors consist of a  $2048 \times 4096$  pixel Hamamatsu Photonics fully depleted back-illuminated CCD with a pixel scale of  $15 \mu\text{m}$  for optical channel and a  $2048 \times 2048$  pixel Raytheon VIRGO-2K HgCdTe array with a pixel scale of  $20 \mu\text{m}$  for infrared channel, respectively (Akitaya et al. 2014). MSI enables optical polarimetric measurements using the EM-CCD camera (Hamamatsu Photonics C9100-13), which employs a back-thinned  $512 \times 512$  pixel frame transfer CCD with a pixel scale of  $16 \mu\text{m}$  (Watanabe et al. 2012). We observed 209P with HONIR/Kanata and MSI/Pirka at large phase angles, that is,  $85.5\text{--}99.5^\circ$  ( $R_C$ -band) and  $85.5\text{--}89.9^\circ$  (J-band). We employed a non-sidereal (cometary motion) tracking with MSI/Pirka, and a sidereal tracking with HONIR/Kanata. The exposure times were chosen ranging from 45 seconds to 180 seconds depending on the detected fluxes and the apparent motion of 209P. Note that the apparent motion of the comet was fast in late May 2014 ( $5\text{--}7'' \text{ min}^{-1}$  with respect to the sidereal tracking) so that we chose short exposure times to reduce the risk of tracking errors of these telescopes. Details of those observations are summarized in Table 1.

### 2.2. Data Reductions

Observed raw data were processed in the standard manner for astronomical imaging data. All object frames were bias subtracted, flat fielded, and cosmic ray corrected using the IRAF reduction package. Figure 1 shows the processed images, which are produced by summing up the reduced ordinary images. We found that the cometary tail was faint in the image on UT 2014 April 23 but became obvious in the  $R_C$ -band image in May 2014. The tail extended between the Sun–comet vector and the negative heliocentric velocity vector, which is typical of cometary dust tails (rather than ion tails). On the contrary, the tail was not

detected in the J-band image due to the low S/N ratio. We noticed the comet was slightly stretched in the apparent direction of movement in the image taken with HONIR/Kanata because we could not employ a comet-tracking mode with the Kanata telescope (theoretically, it stretched by  $1.8''$  on May 23,  $2.8''$  on May 1, and  $3.7''$  on May 17, comparable to or slightly larger than the FWHM in HONIR images).

Imaging polarimetric data have often been analyzed to produce the two-dimensional polarization maps (Furusho et al. 1999, 2007; Jones & Gehrz 2000; Hadamcik et al. 2013). However, since the dust tail was too faint to permit us to make a map, we examined the spatial variation of the linear polarization degrees in the following manner: We first extracted individual source fluxes on the ordinary and extraordinary images by means of the IRAF *apphot* task. Each flux was numerically integrated over the desired circular aperture and the sky background was subtracted using the surrounding annulus (i.e. aperture photometry). We set the aperture size ranging from one to five times the full width at half-maximum (FWHM,  $2.6''$ – $3.5''$ ) of 209P. The extracted intensities are used to obtain the Stokes parameters normalized by the intensity,  $Q/I$ , and  $U/I$ , which are given by:

$$\frac{Q}{I} = \left( 1 - \sqrt{\frac{I_{e,0}/I_{o,0}}{I_{e,45}/I_{o,45}}} \right) / \left( 1 + \sqrt{\frac{I_{e,0}/I_{o,0}}{I_{e,45}/I_{o,45}}} \right), \quad (1)$$

and

$$\frac{U}{I} = \left( 1 - \sqrt{\frac{I_{e,22.5}/I_{o,22.5}}{I_{e,67.5}/I_{o,67.5}}} \right) / \left( 1 + \sqrt{\frac{I_{e,22.5}/I_{o,22.5}}{I_{e,67.5}/I_{o,67.5}}} \right), \quad (2)$$

where  $I_{o,\Psi}$  and  $I_{e,\Psi}$  are the ordinary and extraordinary intensities at the half-wave plate angles  $\Psi$  in degree (Kawabata et al. 1999). The degree of linear polarization ( $P$ ) and the position angle of polarization ( $\theta_P$ ) were calculated as

$$P = \sqrt{\left(\frac{Q}{I}\right)^2 + \left(\frac{U}{I}\right)^2}, \quad (3)$$

and

$$\theta_P = \frac{1}{2} \tan^{-1} \left( \frac{U}{Q} \right), \quad (4)$$

respectively (Tinbergen 1996). For each night, we corrected for the instrumental polarization, the polarization bias, and the position angle zero-point using the results for the polarized and unpolarized standard stars. The polarization quantity ( $P_r$ ) and the position angle of the polarization plane ( $\theta_r$ ) referring to the scattering plane (Zellner & Gradie 1976) were expressed as the following:

$$P_r = P \cos(2\theta_r), \quad (5)$$

and

$$\theta_r = \theta_P - (\phi \pm 90^\circ), \quad (6)$$

where  $\phi$  is the position angle of the scattering plane (see Table 1), and the sign inside the bracket is chosen to satisfy  $0^\circ \leq (\phi \pm 90^\circ) \leq 180^\circ$  (Chernova et al. 1993). In Table 2, we summarize the results of the polarization degrees ( $P$  and  $P_r$ ) and the position angles ( $\theta_P$  and  $\theta_r$ ), which are derived from the multiple data sets at each night.

### 2.3. Nuclear Polarization

From this point on, we tried to distinguish the nuclear flux from the coma flux. In general, the optical depth of most cometary comae is small relative to the nucleus. It is unclear for the flux contrast between the nucleus and the coma (Lamy et al. 2004). We chose the data from two nights (UT 2014 May 4 and 19) obtained with Pirka to allow the use of the precise non-sidereal tracking. The radial profiles of 209P were obtained from the co-added frames, which used only ordinary intensities at the four half-wave plate angles. Stellar radial profiles were defined from the standard star images in the same night. These data were converted into the one-dimensional azimuthally averaged surface brightness by the *pradprof* task in IRAF. The profile parameters were determined by the best fit model with the Moffat PSF fitting function (Moffat 1969). The reduced magnitudes of the nucleus on these two nights,  $R=19.92\pm0.26$  mag and  $R=20.02\pm0.26$  mag, were calculated using an empirical formula,  $R=16.24+0.04\alpha$  (Ishiguro et al. 2015). Figure 2 shows the radial profiles 209P (open circles) together with nucleus model (solid line) on these two nights. It is clear that the observed fluxes are dominated by the nucleus at the radial distance within  $\sim 2\times\text{FWHM}$ , while by the coma beyond  $\sim 2\times\text{FWHM}$ .

To distinguish the nuclear polarization degrees from the coma polarization degree, we made a plot of the polarization degrees taken with different aperture sizes with respect to the ratio of the modelled nuclear flux to the observed flux,  $f_{n/c}$  (Figure 3). We considered the error associated not only with the signal-to-noise ratio and the uncertainty in the sky background determination, but also with the uncertainty of the nuclear magnitude model (i.e. 0.26 mag, Ishiguro et al. 2015). In Figure 3, the data with smaller apertures are plotted in the upper right, while the data with larger apertures are plotted in the lower left. This trend implies that the cometary nucleus is more polarized than the coma. In principal, the  $P$ -intercept (i.e.  $f_{n/c}=0$ ) is supposed to approach the coma polarization degree while the intersection with  $f_{n/c}=1$  approaches the nuclear polarization degree. We thus assumed that the data points in Figure 3 can be fitted with a simple linear function,  $P = (P_c - P_n) \times f_{n/c} + P_n$ , where  $P_n$  and  $P_c$  are polarization degrees of the nucleus and coma, respectively, and derived these values by the method of least squares.

### 3. Results

As the result of fitting, we obtained the polarization degree  $P_n=30.3^{+1.4}_{-0.9}\%$  at  $\alpha=92.2^\circ$  and  $P_n=31.0^{+1.0}_{-0.8}\%$  at  $\alpha=99.5^\circ$  for the nucleus, and  $P_c=28.8^{+0.4}_{-0.4}\%$  at  $\alpha=92.2^\circ$  and  $P_c=29.6^{+0.3}_{-0.3}\%$  at  $\alpha=99.5^\circ$  for the coma. A somewhat surprising result may be derived as the polarization degree for the nucleus.

#### 3.1. Positive branch of polarization

In Table 2, the position angle of the strongest electric vectors,  $\theta_P$ , is in good agreement with those of normal vector to the scattering plane projected on the celestial plane,  $\theta_\perp$  (see Table 1) to an accuracy of a few degrees. For a spherical body,  $\theta_P$  is supposed to align to the normal vector of the scattering plane, and therefore,  $\theta_P=\theta_\perp$ . Although the radar image of 209P showed an irregular shape (Howell et al. 2014), such a regional irregularity may be smoothed out by integrating the flux through the disk. These high polarizations for nucleus indicate a light scattering feature on an object a few kilometers in size (2.5 km×3.2 km, Ishiguro et al. 2015). Since the polarization degree for an airless body is primarily controlled by the surface albedos, the low albedo of the nucleus (the geometric albedo  $P_v \sim 0.05$ , Ishiguro et al. 2015) would result in the high polarization degree. However, we are unable to confirm this because of a lack of precedent for such dark airless bodies (typically  $P_v < 0.1$ ).

The following studies were shown potential for becoming the high polarization degree



( $\sim 30\%$ ) of the dark bodies around  $\alpha=95^\circ$ . There are studies of near-nuclear polarization for 2P/Encke ( $P_v=0.05\pm0.02$ , Fernández et al. 2000). High and low polarizations have been reported to  $P=34.9\%\pm1.7\%$  at  $\alpha=94.6^\circ$  ( $P=39.9\%\pm2.9\%$  when corrected for the  $\text{NH}_2$  contamination) in the red domain (662/5.9nm) (Jorkers et al. 2005) and  $P=11\%\pm3\%$  at  $\alpha=92.9^\circ$  in the green domain (526/5.6nm) (Jewitt 2004) respectively. Considering the contamination by the gaseous species, both studies were measured through the narrow band filter for the same appearance. Note the difference that only the spectral gradient is incompletely explained as pointed out by Hadamcik & Levasseur-Regourd (2009). Polarization of dark airless bodies at the high phase angle were obtained  $P=24.5\%\pm4\%$  at  $\alpha=81^\circ$  for the Martian satellites Phobos ( $P_v=0.07$ , Zellner & Capen 1974) and  $P=22\%\pm4\%$  at  $\alpha=74^\circ$  for Deimos ( $P_v=0.07$ , Thomas et al. 1996) in the orange domain (570nm), while these measurements by Mariner-9 may contain significant systematic errors (Noland et al. 1973). Thus, more observations of dark asteroids are needed to investigate the positive polarization at the higher phase angle.

For the coma, such positive polarization with a maximum of  $P_{\text{max}} = 25\text{--}30\%$  around  $\alpha=95^\circ$  in the red domain was reported in previous studies of the high  $P_{\text{max}}$  comets (see Figure 4). Our measurements for the coma are consistent with them. We found from HONIR measurements that the wavelength dependence of the polarization for the mixture of the nucleus and coma was negligibly small, that is,  $P=30\%\pm3\%$  in  $R_C$ -band and  $P=27\%\pm5\%$  in J-band at  $\alpha=89.9^\circ$  with the aperture size of  $1\text{--}3\times\text{FWHM}$ , although the error of the measurement was not good enough to compare with previous studies.

### 3.2. Phase angle dependence of $P$

Figure 4 shows the phase angle dependence of the polarization degrees of the nucleus and coma. For comparison, we show the previous studies for cometary comae at phase angles larger than about  $80^\circ$  and two red continuum lines through the use of the database of comet polarimetry (Kiselev et al. 2005). Our data shows a moderate increase from  $83.5^\circ$  to  $99.5^\circ$  and no clear peak. There are known to be two classes of comets in terms of the maximum polarization  $P_{\text{max}}$ , so-called 'high-polarization comets' and 'low-polarization comets'. Levasseur-Regourd et al. (1996) reported that these two classes of comets have similar polarization properties at  $\alpha < 40^\circ$  but are bifurcated at larger phase angles. The high-polarization comets have the peak polarization  $P_{\text{max}} \sim 25\%\text{--}28\%$  around  $\alpha=90^\circ\text{--}100^\circ$ , while the low-polarization comets have  $P_{\text{max}} \sim 15\%$  around the same phase angle. In addition, Levasseur-Regourd et al. (1996) described the high-polarization comets as tending to be classified as dusty comets, while the low-polarization comets tend to be classified as gassy comets based on optical spectra. However, the latter case was evaluated as a misleading

definition due to the gas contaminations through the broadband filter (Kiselev et al. 2001, 2004; Jewitt 2004). In the near-nucleus region, the polarizations of some low-polarization comets reach to those of high-polarization comets (Kolokolova et al. 2007).

## 4. Discussion

### 4.1. Contamination of gas

First of all, we would like to discuss the contamination of polarization degree by gas emissions. The observed polarization degrees of comets are known to be occasionally contaminated by gas emissions that reduce the observed polarization degree. In fact, gas-rich comets tend to display low polarization degrees probably because of the depolarization of the gas emission (Kiselev et al. 2001). However, we found that the observed spectra of the 209P coma showed no detectable gas emission in the wavelength range in which we deduced the polarization degree. Figure 5 shows the optical spectra on UT 2014 May 27, only about a week after our polarimetric run, taken at the Nishi-Harima Astronomical Observatory with the Medium and Low-dispersion Long-slit Spectrograph (MALLS) attached to the Nayuta 2.0-m telescope. We employed the lowest-resolution grating ( $150 \text{ line mm}^{-1}$ ),  $8''$ -slit, and the order cut filter of WG320, ensuring the available spectrum at the wavelength 500–730 nm with the spectral resolution  $R \sim 90$ . Note that the continuum slope might be affected by insufficient calibration of the flux with the standard star taken at slightly different airmass. We normalized the obtained reflectance spectrum at 550 nm and subtracted the continuum by the spline interpolation. Figure 5 shows the continuum-subtracted spectrum with the typical emission lines labelled (Brown et al. 1996).

There are clearly no detectable emission lines in the coverage of our  $R_C$  filter, dispelling the gas contamination. Similar results are reported through spectroscopic observation on UT 2014 April 9 that a spectrum in the 350–600 nm range reveals no CN,  $C_2$ , or  $C_3$  emission features (Schleicher 2014). Although there might be time variation in the intensity of gas emission, we conjecture that the variation would be small in our polarimetric data because the  $R_C$ -band monitoring magnitudes did not change over this period (Ishiguro et al. 2015).

We distinguished the polarization of the nucleus  $P_n=30\text{--}31\%$  from that of the coma  $P_c=29\text{--}30\%$  taking account of the signal with different apertures (see Section 2.3). These two values are not necessarily the same, because we observe the scattered light from the coma dust grains in the former, while we observe the reflected light from a kilometer-sized body in the latter. As shown in Figure 4, a comparison between observations performed in other comets indicates a lower trend for the coma polarizations of 209P. We may nevertheless

underestimate the polarization degrees for the coma due to a very slight gas contamination.

#### 4.2. Estimation of maximum polarization $P_{\max}$

The polarization of the nucleus ( $P_n$ ) seems to show higher than the coma ( $P_c$ ) but the differences are insignificant to the accuracy of our measurement. Figure 6 compares the polarization degrees of the nucleus with those of asteroids at phase angles larger than about  $60^\circ$  from the asteroid polarimetric database (Lupishko 2014). All asteroids in the database show polarization degrees remarkably lower than 209P. The phase-polarization curve of (4179) Tautatis is well studied among these asteroids. Ishiguro et al. (1997) determined the phase angle of the maximum polarization at  $\alpha_{\max}=107^\circ\pm10^\circ$ . Although we cannot determine  $\alpha_{\max}$  of 209P with our measurement, we conjecture that our polarimetric measurement was performed around the maximum polarization degree because both the S-type asteroid and cometary coma show the maximum values around the phase angle we measured. For a better understanding of the polarization properties of the nucleus and coma dust at large phase angles, we derived the  $P_{\max}$  using the Lumme and Muinonen function (Goidet-Devel et al. 1995; Penttilä et al. 2005):

$$P_n = b (\sin \alpha)^{c_1} (\cos (0.5\alpha))^{c_2} \sin (\alpha - \alpha_0), \quad (7)$$

where  $b$ ,  $c_1$ ,  $c_2$  and  $\alpha_0$  are constant parameters. According to Penttilä et al. (2005), parameters  $b$  and  $\alpha_0$  affect the amplitude and slope of polarization and the inversion angle, and the other two parameters, the powers  $c_1$  and  $c_2$ , control shapes the phase curve. Because the phase angle coverage of our data is limited, we first fit the phase-polarization relations for comets or asteroids, and then derived  $P_{\max}$  of 209P. Therefore, assuming that the nucleus was essentially identical to low-albedo asteroids ( $P_v < 0.1$ ), we deduced  $P_{\max}$  of the nucleus is 30.8% at  $\alpha_{\max}$  of  $96^\circ$  with the fitted parameters  $b=34.81\%$ ,  $c_1=0.7838$ ,  $c_2=0.2400$  and  $\alpha_0=17.88^\circ$ . For the coma, assuming that the fitted parameters  $c_1=0.7904$ ,  $c_2=0.2418$  and  $\alpha_0=21.59^\circ$  for high-polarization comets and keeping  $b$  as a free parameter, we deduced  $P_{\max}$  of the coma is 29.6% with  $\alpha_{\max}=98^\circ$ .

Our  $P_{\max}$  values are higher polarization than other high-polarization comets and known airless bodies. It was suggested that the presence of jets and arcs in the ambient coma correlated with regions of higher polarization (Tozzi et al. 1997; Furusho et al. 1999; Hadamcik et al. 1997). However, according to Ishiguro et al. (2015), such structures were not identified for 209P. Trends are shown as that are similar to the case with cometary nuclei split into fragments (e.g. C/1999 S4 (Hadamcik & Lvasseur-Regourd 2003c) and 73P (Bonev et al.

2008)), whereas 209P is obvious without such an outburst. Therefore the correlation between cometary activity and polarization excess are considered to be unsuitable for 209P. Some physical properties such as grain size distribution and porosity (Hanner 2003; Hadamcik et al. 2002, 2006) may enhance the polarization degree of 209P, although we have no observational evidence to study these properties.

### 4.3. Comparison with asteroids and slope-albedo relationship

Asteroids show a similar trend of the phase-polarization relation having the maximum polarization at  $\alpha=90^\circ\text{--}120^\circ$  (Ishiguro et al. 1997; Kiselev et al. 1999) but the polarization degrees of these asteroids are significantly lower than that of the 209P nucleus (see Figure 6). Note that only a few asteroids including (1685) Toro, (4179) Toutatis (214869) 2007 PA<sub>8</sub> were observed at large phase angles and they are classified as S-type asteroids. The S-type asteroids show very similar phase-polarization relations. Unique data concerning E-type asteroids, which was obtained from (33342) 1998 WT<sub>24</sub>, indicated  $P_{\max}$  at  $\alpha=72^\circ$  (Kiselev et al. 2002). The linear polarization of (2100) Ra-Shalom (C-type) was measured up to a moderate phase angle ( $\alpha=50^\circ$ ). The C-type asteroid shows large  $P$  at  $\alpha \gtrsim 20^\circ$ , although  $P_{\max}$  for C-type asteroids has not been determined yet. Since S-type asteroids generally have albedos larger than those of C-type asteroids and E-type asteroids have albedos larger than others, it seems that  $P_{\max}$  for asteroids would have a correlation between albedo and  $P_{\max}$ .

A slope of the linear region at the inversion angle  $h$  (as the solid line in Figure 6 shows) was derived as  $0.30\%/^\circ \pm 0.01\%/^\circ$  from the phase-polarization curve. This polarimetric slope  $h$  was slightly steeper than the mean value of C-type objects ( $0.282\%/^\circ \pm 0.025\%/^\circ$ , Gil-Hutton & Canada-Assandri 2012). The relation between the geometric albedo  $P_v$  and the slope  $h$  has been found from the studies of the scattering properties (Zellner et al. 1974; Dollfus et al. 1989; Cellino et al. 1999), and is the following:

$$\log P_v = C_1 \log h + C_2 \quad , \quad (8)$$

where  $C_1$  and  $C_2$  are the constants. These recent values were presented as  $C_1=-1.207 \pm 0.067$  and  $C_2=-1.892 \pm 0.141$  by Masiero et al. (2012). The geometric albedo for the nucleus of 209P is calculated  $0.05^{+0.03}_{-0.02}$  on these constraints, which are consistent findings for Ishiguro et al. (2015) and  $0.049 \pm 0.020$  as the average albedo of the potential dormant comets (Kim et al. 2014).

#### 4.4. $P_{\max}$ -albedo relationship

This  $P_{\max}$ -albedo relationship has long been known as the Umov law. Since the effect is observed on the Moon, Mercury and Mars, the Umov law could essentially be applicable to asteroids and comets. The law is described as (Dollfus 1998):

$$P_{\max} = C_3 (d) P_v^{-C_4} , \quad (9)$$

where  $P_v$  is the geometric albedo.  $C_3$  is a constant, originally proposed  $C_4=1$  by Umov. Also,  $C_3 (d)$  depends a grain size  $d$  of the regolith.

Dollfus (1998) investigated how  $C_3$  and  $C_4$  change according to the grain size. Figure 7 shows the albedo v.s.  $P_{\max}$  plot of 209P together with the Umov function modified by Dollfus (1998) and Shevchenko & Skobeleva (1995). The geometric albedo of 209P was unknown, so we adopted  $0.05^{+0.03}_{-0.02}$  as the likely estimate from Equation (8). We also plotted the data of (1685) Toro, (4179) Tautatis, (33342) 1998 WT<sub>24</sub>, (214869) 2007 PA<sub>8</sub> referring to the geometric albedo of  $0.29 \pm 0.13$  (Masiero et al. 2012),  $0.32 \pm 0.11$  (Kraemer, et al. 2005),  $0.56 \pm 0.20$  (Harris et al. 2007), and  $0.29 \pm 0.09$  respectively. It is likely the albedo- $P_{\max}$  relation can be explained by the Umov law. Although the errors of albedos are too large to enable the regolith sizes on these bodies to be determined, we can safely say that our 209P data favours large ( $\gg 1 \mu\text{m}$ ) particle sizes. Submicron-sized particles were probably well accommodated by gas outflow and lost over time by repeated comet activities.

### 5. Summary

We made polarimetric observations of the highly dormant Jupiter-Family Comet, 209P, at R<sub>C</sub> and J-band during the perihelion passage in 2014 and found the following:

1. No significant difference was found in R<sub>C</sub>- and J-band.
2. Both nucleus and dust coma show high linear polarization degree, that is,  $P_n = 30.3^{+1.3}_{-0.9}\%$  at  $\alpha = 92.2^\circ$  and  $P_n = 31.0^{+1.0}_{-0.7}\%$  at  $\alpha = 99.5^\circ$  for the nucleus, and  $P_c = 28.8^{+0.4}_{-0.4}\%$  at  $\alpha = 92.2^\circ$  and  $29.6^{+0.3}_{-0.3}\%$  at  $\alpha = 99.5^\circ$  for the coma.
3. We detected no significant variation in  $P$  at the phase angle coverage, suggesting that the obtained  $P$  is nearly at maximum in the phase-polarization curves. We deduced  $P_{\max} = 30.8\%$  (nucleus) and  $29.6\%$  (coma), respectively.
4. High  $P_{\max}$  value of the dust coma is consistent with a polarization classification scheme described by Levasseur-Regourd et al. (1996).

5. We employed an empirical function for relating  $P_{\max}$  of the nucleus to the albedo, and found that we obtained a good estimate of the albedo when we assumed the effective size of the regolith particles of  $\approx 1\text{--}100\mu\text{m}$ . The Umov law seems to work on the cometary nuclei as well as the well-studied lunar surface.

### Acknowledgments

We thank an anonymous referee for helpful comments. This work was supported by the Optical and Near-infrared Astronomy Inter-University Cooperation Program and Grants-in-Aid for Scientific Research (23340048, 24000004, 24244014, and 24840031) from the Ministry of Education, Culture, Sports, Science and Technology of Japan. MI was supported by a National Research Foundation of Korea (NRF) grant funded by the Korean government (MEST) (No. 2012R1A4A1028713). SH was supported by the Space Plasma Laboratory, ISAS, JAXA (the Hypervelocity Impact Facility).

### REFERENCES

- Akitaya, H., Moritani, Y., Ui, T., et al. 2014, Proc. SPIE, 9147, 91474O
- Bagnulo S., Tozzi G.P., Boehnhardt H., et al. 2010, A&A, 514, 1
- Belskaya I. N., Levasseur-Regourd A.-C., Cellino A. et al. 2009, Soviet Ast., 199, 97
- Belskaya I. N., Lupishko D. F., & Shakhovskoj N. M. 1987, Soviet Ast., 13, 219
- Belskaya I. N., Shkuratov Yu. G., Efimov Yu. S. et al. 2005, Icarus, 178, 213
- Bonev, T., Boehnhardt, H. & Borisov, G. 2008, A&A, 480, 277
- Brown, P. 2014, Central Bureau Electronic Telegrams, 3886, 1
- Brown, M. E., Bouchez, A. H., Spinrad, A. H., & Johns-Krull, C. M. 1996, AJ, 112, 1197
- Canada-Assandri M., Gil-Hutton R., & Benavidez P. 2012, 542, A11
- Cellino, A., Hutton, R. Gil, Tedesco, E. F., et al. 1999, Icarus, 138, 129
- Cellino, A., Yoshida, F., Anderlucci, E., et al. 2005, Icarus, 179, 297
- Chernova, G. P., Kiselev, N.N., & Jockers, K. 1993, Icarus, 103, 133

- Dollfus, A., Wolff, M., Geake, J. E., Dougherty, L. M., & Lupishko, D. F. 1989, *Asteroids II*, 594
- Dollfus, A. 1998, *Icarus*, 136, 69
- Eaton, N., Scarrott, S. M., Warren-Smith, R. F. 1988, *Icarus*, 76, 270
- Eaton, N., Scarrott, S. M., Gledhill, N. M. 1992, *MNRAS*, 258, 384
- Fernández, Y. R., Lisse, C. M., Ulrich Käußl, H., et al. 2000, *Icarus*, 147, 145
- Fornasier, S., Belskaya, I. N., & Perna, D. 2015, *Icarus*, 250, 280
- Fornasier S., Belskaya I., Shkuratov Yu.G., et al., 2006, *Icarus*, 455, 371
- Furusho, R., Suzuki, B., Yamamoto, N., et al. 1999, *PASJ*, 51, 367
- Furusho, R., Ikeda, Y., Kinoshita, D., et al. 2007, *Icarus*, 190, 454
- Ganesh, S., Joshi, U. C., Baliyan, K. S. 2009, *Icarus*, 201, 666
- Gil-Hutton, R. & Canada-Assandri, M. 2012, *A&A*, 539, A115
- Gil-Hutton, R., Cellino, A., & Bendjoya, P. 2014, *A&A*, 569, AA122
- Goidet-Devel, B., Renard, J. B., & Levasseur-Regourd, A. C. 1995, *Planet. Space Sci.*, 43, 779
- Hadamcik, E., & Levasseur-Regourd, A. C. 2003, *J. Quant. Spec. Radiat. Transf.*, 79-80, 679
- Hadamcik, E., & Levasseur-Regourd, A. C. 2003, *A&A*, 403, 757
- Hadamcik, E., & Levasseur-Regourd, A. C. 2003, *Icarus*, 166, 188
- Hadamcik, E., & Levasseur-Regourd, A. C. 2009, *Planet. Space Sci.*, 57, 1118
- Hadamcik, E., Levasseur-Regourd, A. C., & Renard, J. B. 1997, *Earth, Moon, and Planets*, 78, 365
- Hadamcik, E., Renard, J. B., Levasseur-Regourd, A. C. et al., 2006, *J. Quant. Spec. Radiat. Transf.*, 100, 143
- Hadamcik, E., Renard, J. B., Worms, J. C., et al., 2002, *Icarus*, 155, 497
- Hadamcik, E., Sen, A. K., Levasseur-Regourd, A. C., et al. 2013, *Icarus*, 222, 774



- Hanner, M., 2003, *J. Quant. Spec. Radiat. Transf.*, 79-80, 695
- Harris, A. W., Mueller, M., Delbó, M., et al. 2007, *Icarus*, 188, 414
- Hergenrother, C. 2014, *Central Bureau Electronic Telegrams*, 3870, 1
- Howell, E. S., Nolan, M. C., Taylor, P. A., et al. 2014, *AAS/Division for Planetary Sciences Meeting Abstracts*, 46, #209.24
- Ishiguro, M., Kuroda, D., Hanayama, H., et al. 2015, *ApJ*, 798, L34
- Ishiguro, M., Nakayama, H., Kogachi, M., et al. 1997, *PASJ*, 49, L31
- Jenniskens, P., & Lyytinen, E. 2014, *Central Bureau Electronic Telegrams*, 3869, 1
- Jewitt, D. 2004, *AJ*, 128, 3061
- Jockers, K., Kiselev, N., Bonev, T., et al. *A&A*, 441, 773
- Jones, T. J., & Gehrz, R. D. 2000, *Icarus*, 143, 338
- Joshi, U. C., Baliyan, K. S., Ganesh, S. 2003, *A&A*, 405, 1129
- Kraemer, K. E., Lisse, C. M., Price, Stephan D., et al. 2005, *AJ*, 130, 2263
- Kawabata, K. S., Okazaki, A., Akitaya., H., et al. 1999, *PASP*, 111, 898
- Kikuchi, S. 2006, *J. Quant. Spec. Radiat. Transf.*, 100, 179
- Kikuchi, S., Mikami, Y., Mukai, T., et al. 1987, *A&A*, 187, 689
- Kikuchi, S., Mikami, Y., Mukai, T., et al. 1989, *A&A*, 214, 386
- Kim, Y., Ishiguro, M., Usui, F. 2014, *ApJ*, 789, 151
- Kiselev, N. N., Chernova, G. P. 1978, *Soviet Astronomy Letters*, 55, 1064
- Kiselev, N. N., Jockers, K., & Bonevc, T. 2001, *Solar System Research*, 35, 480
- Kiselev, N. N., Jockers, K., Rosenbush, V. K., & Korsun, P. P. 2001, *Solar System Research*, 35, 480
- Kiselev, N. N., Lupishko, D. F., Chernova, G. P., et al. 1990, *Kinematika i Fizika Nebesnykh Tel*, 6, 77
- Kiselev, N. N., Rosenbush, V. K., & Jockers, K. 1999, *Icarus*, 140, 464



- Kiselev, N. N., Rosenbush, V. K., Jockers K., et al. 2002, in: Proceedings of Asteroids, Comets, Meteors - ACM 2002 ed. B. Warmbein (Berlin, Germany : ESA SP-500), 887
- Kiselev, N., Velichko, S., Jockers, K., et al. 2005, *Earth, Moon, and Planets*, 97, 365
- Kolokolova, L., Kimura, H., Kiselev, N., & Rosenbush, V. 2007, *A&A*, 463, 1189
- Lamy, P. L., Toth, I., Fernandez, Y. R., & Weaver, H. A. 2004, *Comets II*, 223
- Levasseur-Regourd, A. C., Hadamcik, E., & Renard, J. B. 1996, *A&A*, 313, 327
- Lumme, K., & Muinonen, K. O. 1993, *LPI Contributions*, 810, 194
- Lupishko, D. 2014, *NASA Planetary Data System*, 215,
- Lupishko D. F., Kiselev N. N., Chernova G. P., et al. 1994, *Kinematika Fiz. Nebesn. Tel.*, 10, 40-44
- Masiero, J. R., Mainzer, A. K., Grav, T., et al. 2012, *ApJ*, 749, 104
- Michalsky J. J. 1981, *Icarus*, 47, 388
- Moffat, A. F. J. 1969, *A&A*, 3, 455
- Mukai, T., Iwata, T., Kikuchi, S., et al. 1997, *Icarus*, 127, 452
- Myers, R. V. 1985, *Icarus*, 63, 206
- Nakayama H., Fujii Y., Ishiguro M., et al. 2000, *Icarus*, 146, 220-231
- Noland, M., Veverka, J., & Pollack, J. B. 1973, *Icarus*, 20, 490
- Penttilä, A., Lumme, K., Hadamcik, E., et al. 2005, *A&A*, 432, 1081
- Rosenbush, V. K., Rosenbush A. E., Dement'ev M. S. 1994, *Icarus*, 108, 81
- Schleicher, D. 2014, *Central Bureau Electronic Telegrams*, 3880, 1
- Shkuratov, Y., Ovcharenko, A., Zubko, E., et al. 2002, *Icarus*, 159, 396
- Shevchenko, V. V., & Skobeleva, T. P. 1995, *Solar System Research*, 29, 74
- Tinbergen, J. 1996, *Astronomical Polarimetry* (Cambridge University Press), iSBN: 0521475317

- Thomas, P. C., Adinolfi, D., Helfenstein, P., et al. 1996, *Icarus*, 123, 536
- Tozzi, G. P., Cimatti, A., di Serego Alighieri, S., et al. 1997, *Planet. Space Sci.*, 45, 535
- Watanabe, M., Takahashi, Y., Sato, M., et al. 2012, *Proc. SPIE*, 8446, 84462O
- Zellner, B., & Capen, R. C. 1974, *Icarus*, 23, 437
- Gehrels T., & Gradie J. 1974, *AJ*, 79, 1100
- Zellner, B., & Gradie J. 1976, *AJ*, 81, 262
- Zubko, E., Furusho, R., Kawabata, K., et al. 2011, *J. Quant. Spec. Radiat. Transf.*, 112, 1848

Table 1. Observational circumstances.

Date	UT	Filter	$Exp^{(a)}$	$N^{(b)}$	$r^{(c)}$	$\Delta^{(d)}$	$\alpha^{(e)}$	$\theta_{\perp}^{(f)}$	$\phi^{(g)}$	Inst. <sup>(h)</sup>
2014/04/23	12:21-13:43	R <sub>C</sub>	132	12	0.987	0.335	83.5	1.3	91.3	HONIR
2014/04/23	12:21-13:43	J	120	12	0.987	0.335	83.5	1.3	91.3	HONIR
2014/05/01	13:01-13:48	R <sub>C</sub>	132	12	0.972	0.268	89.9	2.4	92.4	HONIR
2014/05/01	13:01-13:48	J	120	12	0.972	0.268	89.9	2.4	92.4	HONIR
2014/05/04	13:04-14:31	R <sub>C</sub>	180	24	0.970	0.242	92.2	3.2	93.2	MSI
2014/05/17	12:23-14:29	R <sub>C</sub>	45	54	0.983	0.127	99.4	10.2	100.2	HONIR
2014/05/19	11:23-12:09	R <sub>C</sub>	60	36	0.988	0.110	99.5	12.2	102.2	MSI

<sup>(a)</sup>Individual effective exposure time in seconds.

<sup>(b)</sup>Number of exposures.

<sup>(c)</sup>Median heliocentric distance in AU.

<sup>(d)</sup>Median geocentric distance in AU.

<sup>(e)</sup>Median Solar phase angle (Sun–209P–Observer angle) in degree.

<sup>(f)</sup>Median position angle of normal vector with respect to the scattering plane in degree.

<sup>(g)</sup>Median position angle of the scattering plane in degree.

<sup>(h)</sup>Employed instruments.

Table 2. Degree of linear polarization and position angle of polarization for 209P

Date	Filter	$A_p^{(a)}$	$P^{(b)}$	$\sigma P^{(c)}$	$\theta_P^{(d)}$	$\sigma\theta_P^{(e)}$	$P_r^{(f)}$	$\theta_r^{(g)}$
2014/04/23	R <sub>C</sub>	3.03	30.7	3.0	3.9	2.8	30.6	2.6
2014/04/23	R <sub>C</sub>	6.06	25.3	1.1	179.4	1.2	25.2	178.1
2014/04/23	R <sub>C</sub>	9.09	27.8	4.8	2.2	4.9	27.8	0.9
2014/04/23	R <sub>C</sub>	12.12	25.6	3.6	176.8	4.1	25.3	175.5
2014/04/23	R <sub>C</sub>	15.15	21.2	7.4	172.4	52.0	20.2	171.1
2014/04/23	J	2.59	33.8	2.2	1.5	1.8	33.8	0.2
2014/04/23	J	5.18	31.7	5.5	0.7	5.0	31.7	-0.6
2014/04/23	J	7.77	30.5	5.5	176.4	5.1	30.1	175.1
2014/04/23	J	10.36	26.3	3.3	172.9	3.5	25.2	171.6
2014/04/23	J	12.95	20.6	4.1	1.3	5.7	20.6	0.0
2014/05/01	R <sub>C</sub>	2.84	30.5	0.6	5.7	0.5	30.3	3.3
2014/05/01	R <sub>C</sub>	7.06	32.1	3.4	1.5	3.1	32.1	-0.9
2014/05/01	R <sub>C</sub>	10.59	28.5	5.8	3.5	5.8	28.5	1.1
2014/05/01	R <sub>C</sub>	14.12	36.2	6.4	179.3	5.0	36.0	176.9
2014/05/01	R <sub>C</sub>	17.65	18.5	8.8	6.7	52.0	18.3	4.3
2014/05/01	J	2.61	30.2	5.0	175.3	4.7	29.3	172.9
2014/05/01	J	5.22	27.1	2.3	1.9	2.4	27.1	-0.5
2014/05/01	J	7.83	23.8	6.5	4.6	7.9	23.7	2.2
2014/05/01	J	10.44	23.5	4.6	9.7	5.6	22.7	7.3
2014/05/01	J	13.05	20.9	4.6	177.9	6.3	20.6	175.5
2014/05/04	R <sub>C</sub>	3.53	30.12	0.18	2.01	0.21	30.10	-1.16
2014/05/04	R <sub>C</sub>	7.06	29.95	0.23	1.64	0.26	29.91	-1.53
2014/05/04	R <sub>C</sub>	10.59	29.62	0.24	1.41	0.27	29.56	-1.76
2014/05/04	R <sub>C</sub>	14.12	29.42	0.27	1.42	0.29	29.37	-1.75
2014/05/04	R <sub>C</sub>	17.65	29.86	0.35	1.40	0.36	29.80	-1.77
2014/05/17	R <sub>C</sub>	3.53	35.2	4.0	10.0	3.2	35.2	-0.2
2014/05/17	R <sub>C</sub>	7.06	37.3	6.8	10.8	5.2	37.3	0.6
2014/05/17	R <sub>C</sub>	10.59	30.3	1.9	6.1	1.8	30.0	-4.1
2014/05/17	R <sub>C</sub>	14.12	36.3	3.8	6.0	3.0	35.9	-4.2
2014/05/17	R <sub>C</sub>	17.65	32.1	3.5	5.1	3.1	31.6	-5.1
2014/05/19	R <sub>C</sub>	2.79	30.88	0.11	11.06	0.17	30.86	-1.11

Table 2—Continued

Date	Filter	Ap <sup>(a)</sup>	P <sup>(b)</sup>	$\sigma P^{(c)}$	$\theta_P^{(d)}$	$\sigma\theta_P^{(e)}$	$P_r^{(f)}$	$\theta_r^{(g)}$
2014/05/19	R <sub>C</sub>	5.58	30.47	0.12	11.03	0.17	30.45	-1.14
2014/05/19	R <sub>C</sub>	8.37	30.32	0.13	11.05	0.18	30.30	-1.12
2014/05/19	R <sub>C</sub>	11.16	30.35	0.14	10.99	0.18	30.32	-1.18
2014/05/19	R <sub>C</sub>	13.95	30.41	0.17	10.94	0.20	30.38	-1.23

<sup>(a)</sup>Aperture radius in arcsec.

<sup>(b)</sup>Polarization degree in percent.

<sup>(c)</sup>Standard deviation of  $P$  in percent.

<sup>(d)</sup>Position angle of the strongest electric vector in degree.

<sup>(e)</sup>Standard deviation of  $\theta_P$  in degree.

<sup>(f)</sup>Polarization degree referred to the scattering plane in percent.

<sup>(g)</sup>Position angle referred to the scattering plane in degree.

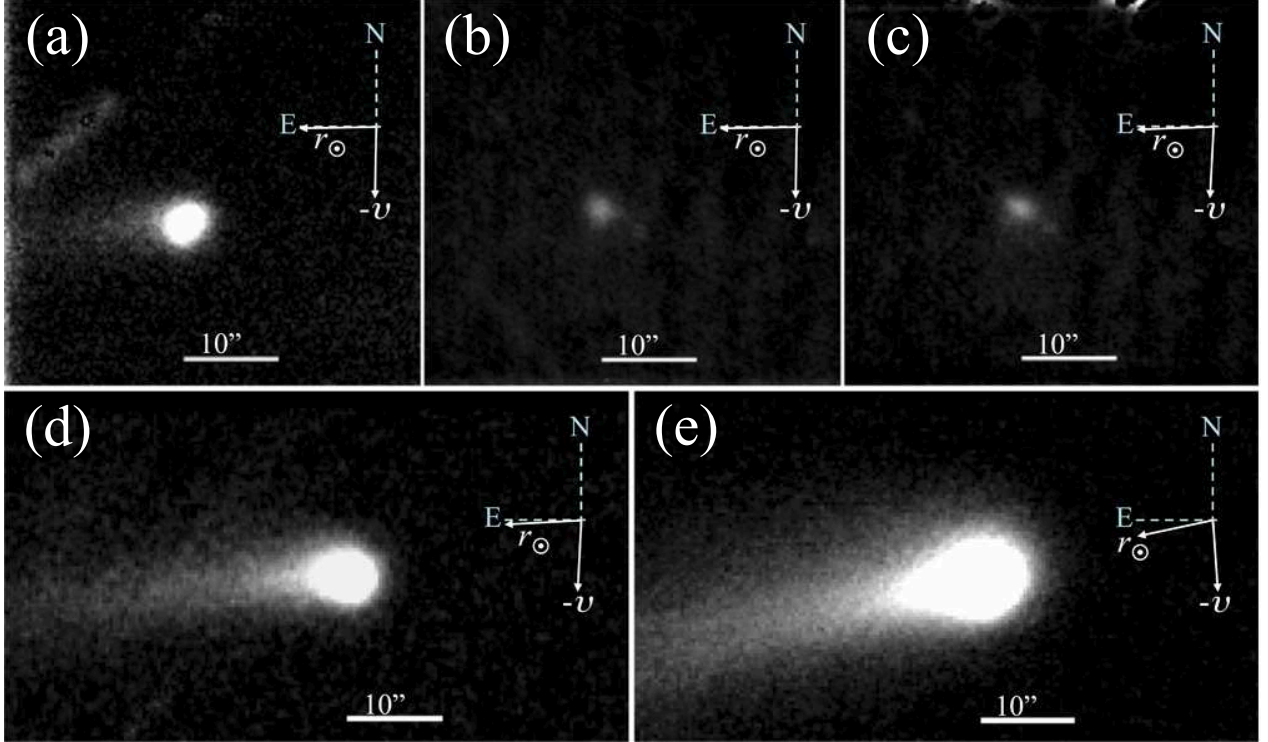


Fig. 1.— Optical and near-infrared ordinary images of 209P taken on (a) UT 2014 April 23 with HONIR in  $R_C$ -band, (b) UT 2014 April 23 with HONIR in J-band, (c) UT 2014 May 1 with HONIR in J-band, (d) UT 2014 May 4 with MSI in  $R_C$ -band, and (e) UT 2014 May 17 with MSI in  $R_C$ -band. The comet nucleus is located at the center of each panel. The Celestial North is up and Celestial East to the left. (a)–(c) have the field-of-view of  $44'' \times 41''$  and (d)–(e)  $67'' \times 38''$ . The Sun $\rightarrow$ 209P vector ( $r_\odot$ ) and the negative heliocentric velocity vector ( $-v$ ) are shown by arrows.

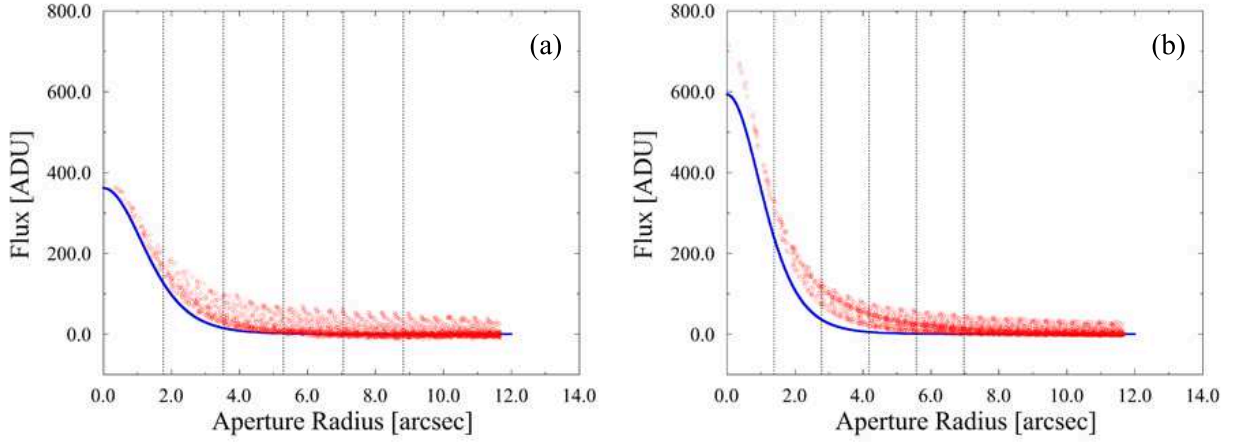


Fig. 2.— Radial profiles in the ordinary images from observations made on (a) UT 2014 May 4 and (b) UT 2014 May 19 using MSI in  $R_C$ -band. The open circles show the extracted data points as the radial profile of 209P. The solid line shows the point-spread-function of the star scaled to the nuclear flux. The vertical dotted lines correspond to  $1\text{--}5\times\text{FWHM}$  of the comet. From the comparison, it is obvious the nuclear flux is dominated at smaller distance (within  $\sim 2\times\text{FWHM}$ ) while coma flux dominates at a greater distance (beyond  $\sim 2\times\text{FWHM}$ )

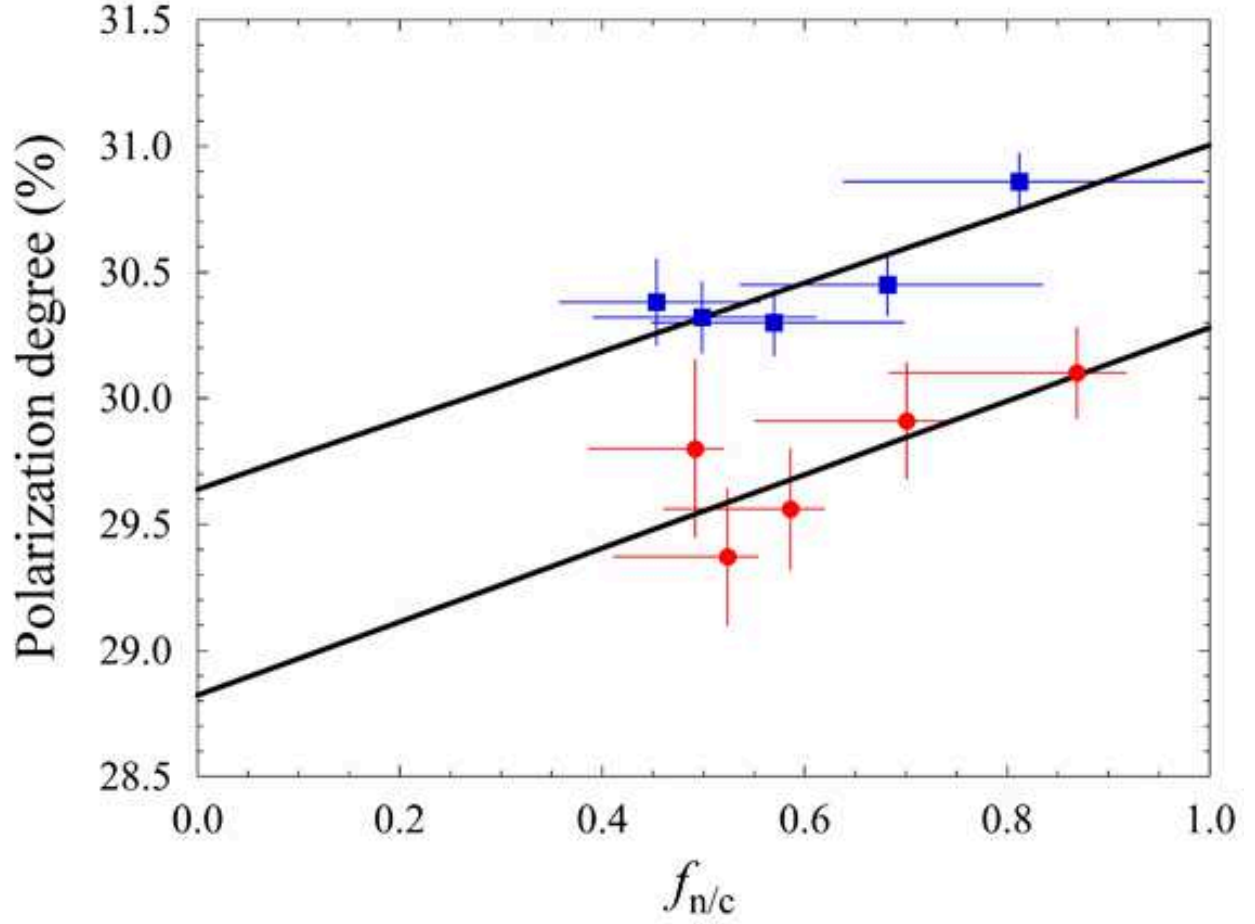


Fig. 3.— Polarization degree ( $P$ ) with respect to ratio of the nuclear flux to the observed flux  $f_{n/c}$  taken on UT 2014 May 4 (filled circles) and 19 (filled squares). The solid lines are fitted ones for  $P$ – $f_{n/c}$  plots on each night. The intercept along the vertical axis (i.e.  $f_{n/c} = 0$ ) asymptotically approaches the coma polarization degree whereas the intersection with  $f_{n/c}=1$  approximately equals the polarization degree of the nucleus.



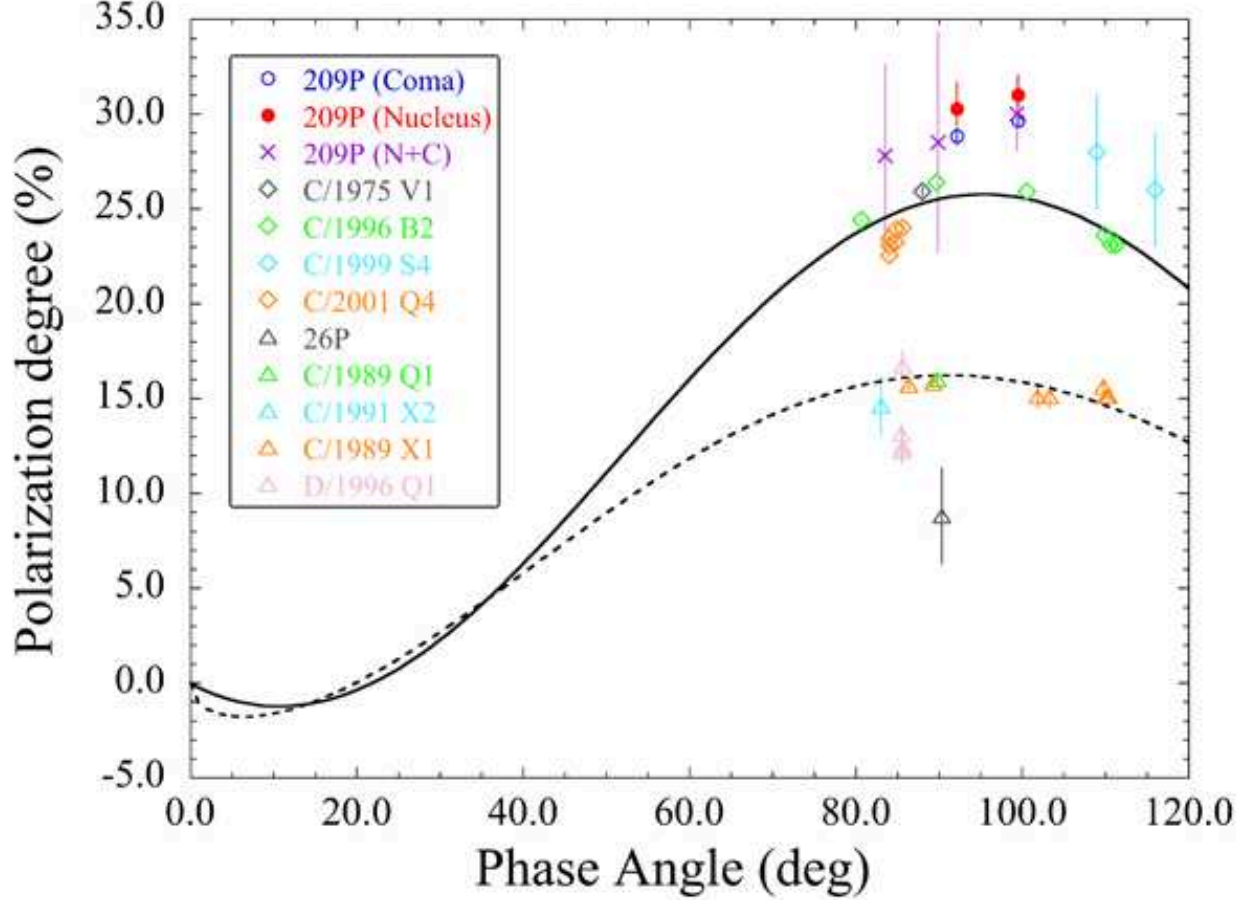


Fig. 4.— Phase angle dependence of polarization for 209P nucleus (filled circles) and coma (open circles) taken with MSI. Regarding data taken with HONIR (indicated by crosses), we adopted blended signals of nucleus and coma with relatively large aperture ( $3\times\text{FWHM}$ ) due to inadequate tracking of the telescope. For comparison, we show polarization degrees of other comets in R-band region (about  $650\pm 50$  nm), which are mostly attributed to light scattered by dust particles in comae. Two fit lines with the Lumme and Muinonen function, high  $P_{\text{max}}$  (solid line and open diamonds) and low  $P_{\text{max}}$  (dashed line and open triangles) comprise the PDS archive (Kiselev & Chernova 1978; Michalsky 1981; Myers 1985; Kikuchi et al. 1987, 1989; Eaton et al. 1988, 1992; Rosenbush et al. 1994; Levasseur-Regourd et al. 1996; Hadamcik & Levasseur-Regourd 2003a,b; Joshi et al. 2003; Kikuchi 2006; Ganesh et al. 2009)

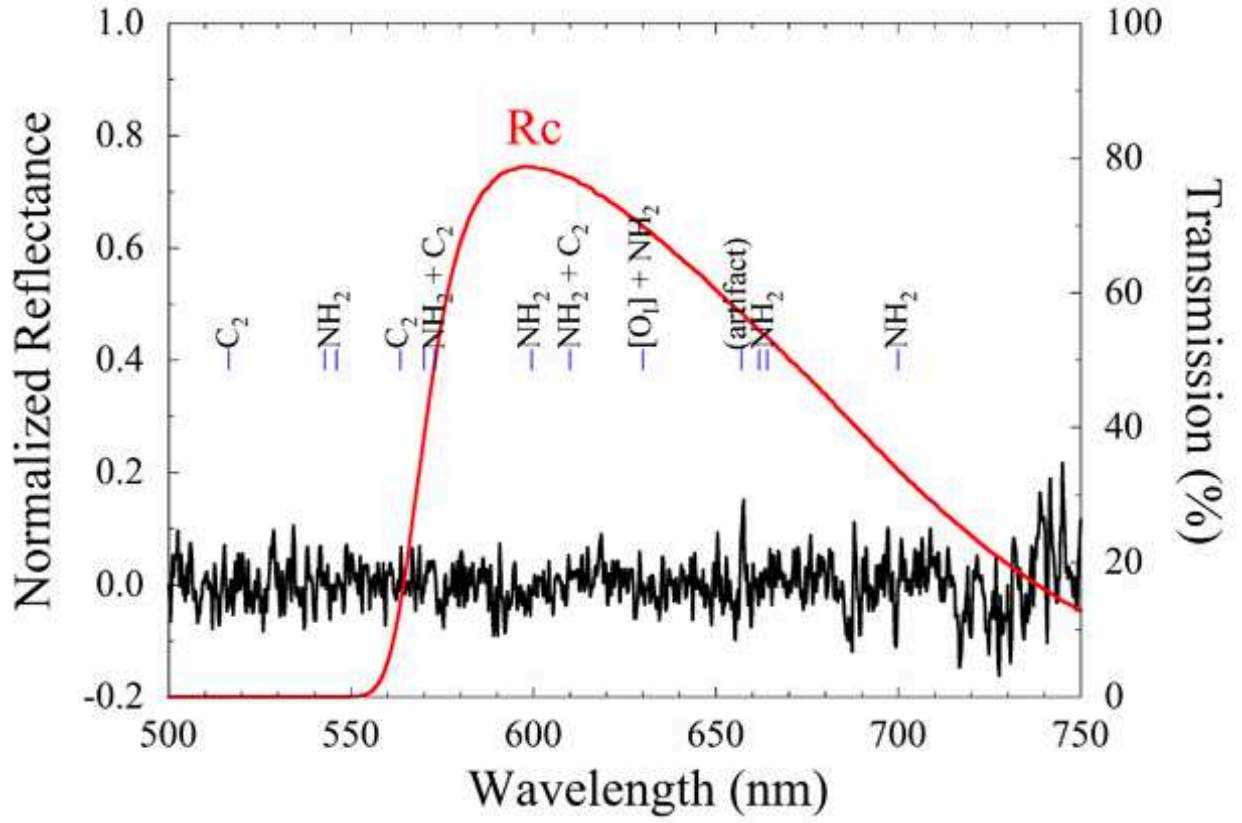


Fig. 5.— Continuum-subtracted spectrum of 209P taken at the Nishi-Harima Astronomical Observatory with MALLS. Major emission lines are labelled and the peak at 658 nm is evaluated as a calibration artifact. The transmission curve of our  $R_C$  filter is indicated too.

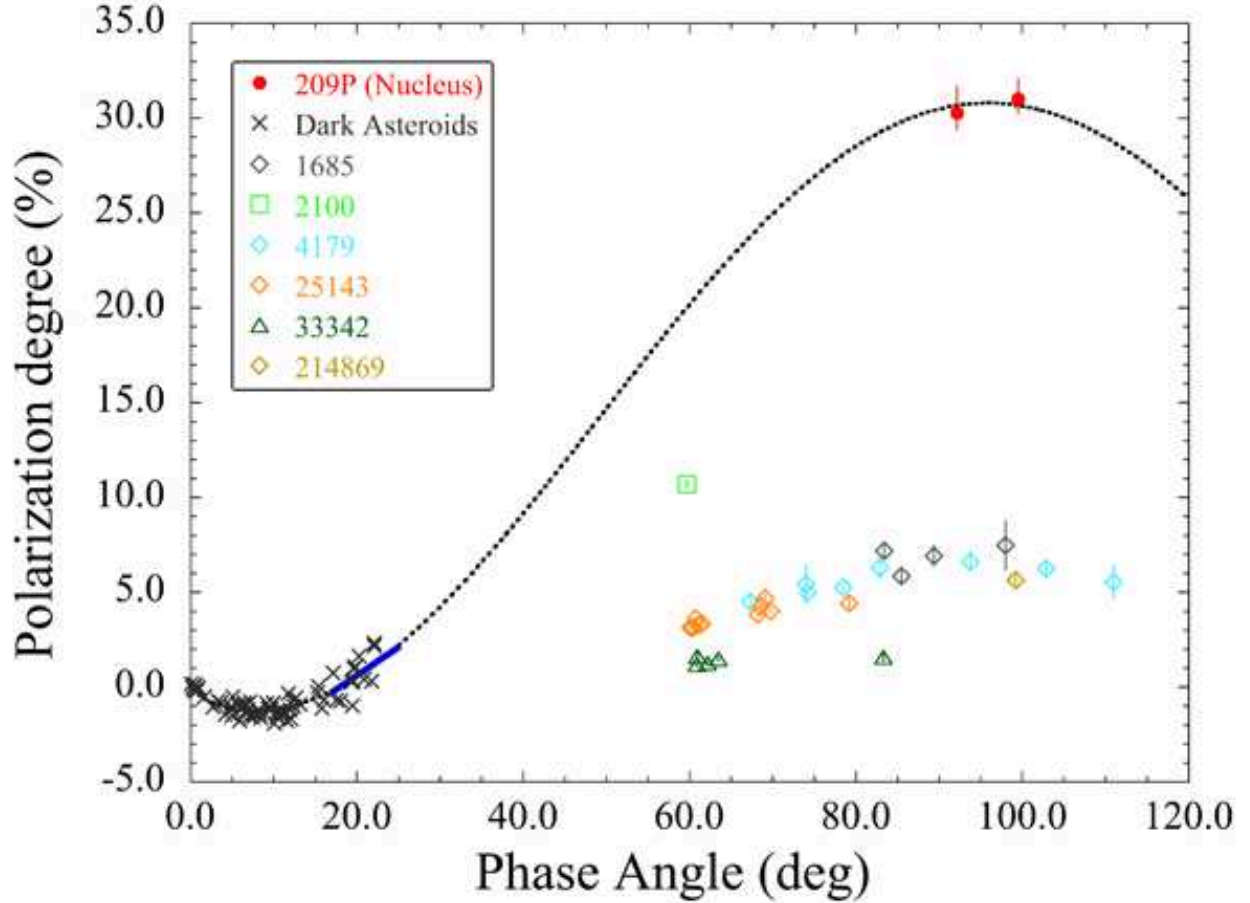


Fig. 6.— Comparison of phase angle dependence of polarization of 209P at  $R_C$ -band, reported in this paper, with those of near-Earth asteroids, 1685 Toro (Kiselev et al. 1990), 4179 Toutatis (Ishiguro et al. 1997; Mukai et al. 1997), 2100 Ra-Shalon (Kiselev et al. 1999), 25143 Itokawa (Cellino et al. 2005), 33342 1998 WT<sub>24</sub> (Kiselev et al. 2002), and 214869 2007 PA<sub>8</sub> (Fornasier et al. 2015). The dotted line is produced by means of the Lumme and Muinonen function between 209P nucleus and the dark asteroids from the PDS archive (Zellner et al. 1974; Belskaya et al. 1987; Nakayama et al. 2000; Belskaya et al. 2005; Fornasier et al. 2006; Belskaya et al. 2009; Bagnulo et al. 2010; Canada-Assandri et al. 2012; Gil-Hutton & Canada-Assandri 2012; Lupishko 2014). The solid line shows a slope of the linear region of the phase-polarization curve.

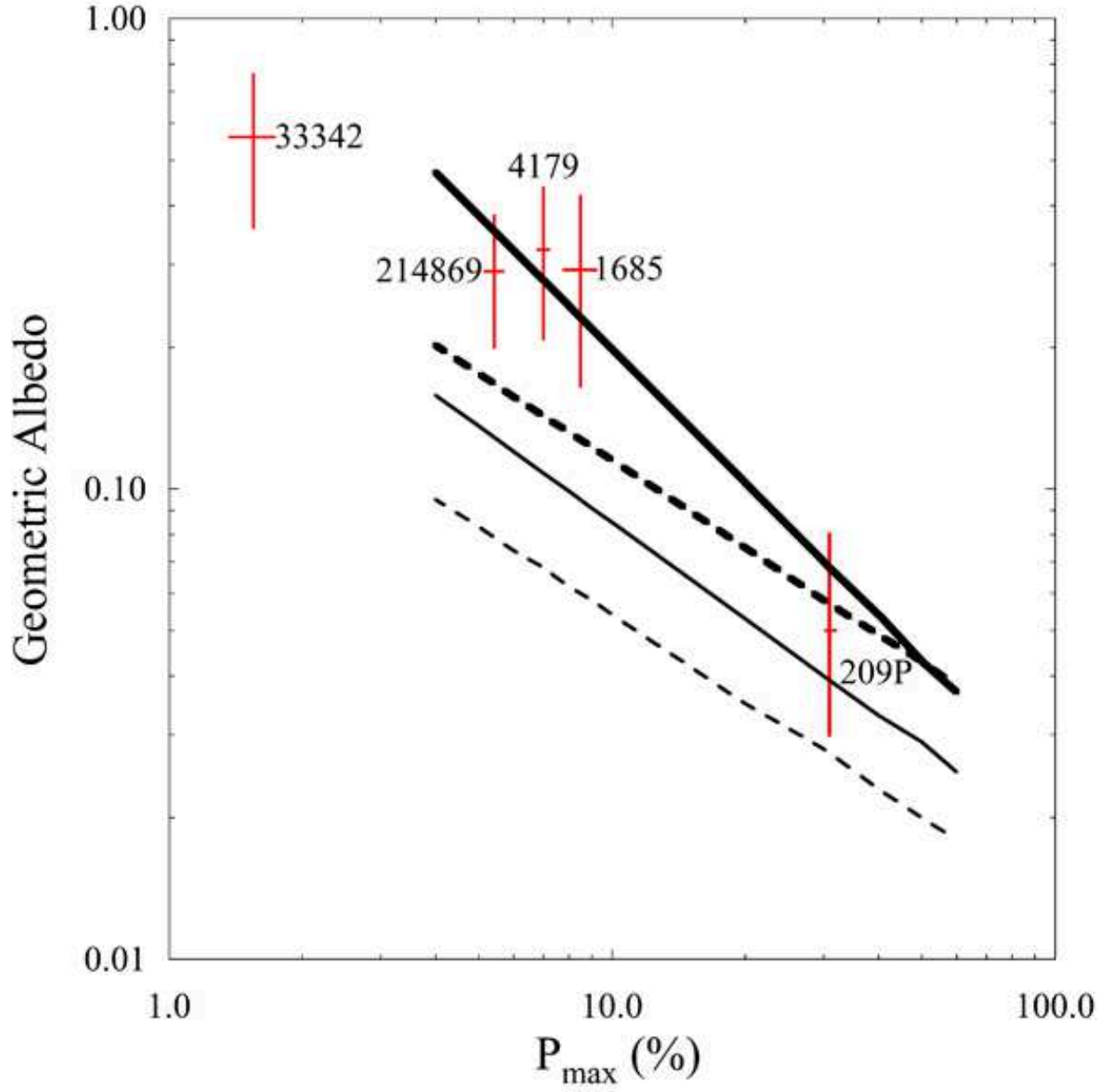


Fig. 7.— Geometric albedo with respect to  $P_{\max}$  for (1685) Toro, (4179) Toutatis (214869) 2007 PA<sub>8</sub> (S-type), (33342) 1998 WT<sub>24</sub> (E-type), and 209P. Albedo –  $P_{\max}$  relations based on two models shown by solid (Dollfus 1998) and dashed lines (Shevchenko & Skobeleva 1995) are plotted as typical surface grain sizes: coarse grain(160  $\mu\text{m}$ ) and fine grain(1-4  $\mu\text{m}$ ). The bold lines are also indicators for the coarse grain.